Microlocal Analysis of Elliptical Radon Transforms with Foci on a Line

Venkateswaran P. Krishnan, Howard Levinson and Eric Todd Quinto

*We dedicate this article to the memory of Leon Ehrenpreis,
a brilliant mathematician and a Mensch.*

Abstract In this paper, we take a microlocal approach to the study of an integral geometric problem involving integrals of a function on the plane over 2-dimensional sets of ellipses on the plane. We focus on two cases: (a) the family of ellipses where one focus is fixed at the origin and the other moves along the x-axis, and (b) the family of ellipses having a common offset geometry.

For case (a), we will characterize the Radon transform as a Fourier integral operator associated to a fold and blowdown. This has implications on how the operator adds singularities, how backprojection reconstructions will show those singularities, and in comparison of the strengths of the original and added singularities in a Sobolev sense.

For case (b) we show that this Radon transform has similar structure to case (a): it is a Fourier integral operator associated to a fold and blowdown. This case is related to previous results of authors one and three. We characterize singularities that are added by the reconstruction operator, and we present reconstructions from the authors' algorithm that illustrate the microlocal properties.

Venkateswaran P. Krishnan
Tata Institute of Fundamental Research Centre for Applicable Mathematics, Bangalore 560065
India e-mail: vkrishnan@math.tifrbng.res.in

Howard Levinson
1759 Beechwood Blvd., Pittsburgh, PA 15217 USA e-mail: howielevinson@gmail.com

Eric Todd Quinto
Tufts University, Medford, MA 02155 USA e-mail: todd.quinto@tufts.edu

1 Introduction

In Synthetic Aperture Radar (SAR) imaging, a region of interest on the surface of the earth is illuminated by electromagnetic waves from a moving airborne platform. The goal is to reconstruct an image of the region based on the measurement of scattered waves. For an in-depth treatment of SAR imaging, we refer the reader to [8, 6]. SAR imaging is similar to other imaging problems such as Sonar where acoustic waves are used to reconstruct the shape of objects on the ocean floor [3].

Depending on the acquisition geometry, the transmitter and the receiver can be located on the same platform (monostatic SAR imaging) or different airborne platforms (bistatic SAR imaging).

There are several advantages to considering bistatic data acquisition geometries. The receivers, compared to the transmitters, are passive and hence are more difficult to detect. Hence, by separating their locations, the receivers alone can be in an unsafe environment, while the transmitters are in a safe environment. Bistatic SAR acquisition geometry arises naturally when imaging using a stationary transmitter such as a television or radio broadcasting station. Finally, bistatic SAR systems are more resistant to electronic countermeasures such as target shaping to reduce scattering in the direction of incident waves [32].

Under certain simplifying assumptions, the scattered data can be viewed as integrals of a function over a family of ellipses in the case of bistatic SAR, compared to a family of circles for the case of monostatic SAR. Thus, imaging using a bistatic SAR system leads to the question of recovering a function given its integrals over a family of ellipses. With this as our motivation, we analyze two elliptical Radon transforms in this paper. In Section 2 we give microlocal properties of the transform that integrates over ellipses with one focus fixed at the origin and the other focus moving on a line. We show using microlocal analysis why there are added singularities in reconstructions. In Section 3 we consider the elliptical transform involving a common offset geometry, where the foci are on a line at a fixed positive distance apart and move along this line. In Section 4 we describe our algorithm and reconstructions from that algorithm. As before, we explain, using microlocal analysis, why there are added singularities in the reconstructions.

Radon transforms over circles and spheres have a rich theory starting from the early 1900s. In 1916, Funk inverted the transform integrating over great circles on the sphere [22]. Then researchers such as John [33], Courant and Hilbert [9], Helgason [30] and many others proved important results for spherical integrals in $\mathbb{R}^n$ and manifolds. The article [58] gives a very readable summary of the large number of themes in the field up to that point. In the article [1], microlocal and harmonic analysis are used to characterize invertibility for the circular Radon transform with centers on a curve.

Our elliptical transform in Section 2 integrates over ellipses that enclose the origin. Helgason [30] proved a support theorem for the transform integrating over spheres in $\mathbb{R}^n$ enclosing the origin under the assumption that the function is rapidly decaying at infinity. Globevnik [23, Theorem 1] characterizes the null space of the Radon transform integrating over circles enclosing the origin.

Leon Ehrenpreis considered spherical Radon transforms in several contexts. For example, [12] is a lovely article involving integrals over spheres tangent to a set, and he discussed spherical integrals in relation to Huygens Principle in his book *The Universality of the Radon Transform* [13, p. 132 ff]. In the book, he applied Radon transforms to PDE, harmonic analysis, and Fourier analysis, as well as tomography and even topics related to number theory. He developed a theory of the nonparametric Radon transform [13, p. 4 ff], and our two elliptic transforms can be put in this framework. We work the details out for case (a) in Example 1.

Less is known about integrals over ellipses. Volchkov [56] and others considered convolution integrals over sets such as ellipsoids. Elliptical integrals come up in ultrasound [2, 54] as well. The sound source and receiver are at different locations and the sound wavefronts are elliptical giving rise to elliptical Radon transforms.

Microlocal analysis has a long history in integral geometry starting with [27, 29, 28]. Then many other authors have applied microlocal analysis to integral geometric problems. A very partial listing of the themes and a few papers in those areas include microlocal properties of the operators and their compositions [46, 25, 26, 53, 52], applications to support theorems and uniqueness [5, 4, 1, 48, 35, 37], applications to SAR imaging [7, 16, 17, 41, 43, 36], and applications to other modalities in tomography including X-ray CT [47, 21, 34], SPECT [50], electron microscopy [51], and seismic imaging [11, 18, 19, 40, 45, 10].

2 Analysis of an Elliptical Radon transform with One Fixed Focus

In this section, we will study the microlocal analysis of an elliptical Radon transform integrating over ellipses in which one focus is fixed at the origin and the other is free to move along the horizontal axis. As explained in the introduction, this acquisition geometry is related to one in SAR imaging. The receiver is passive, often smaller and less expensive to replace than the transmitter. Therefore, in dangerous environments, it might be advantageous to let the transmitter and receiver move independently. One useful case to study is when the receiver can use a radio or cellphone transmitter that is already in the environment. Thus, the radar problem has a fixed transmitter location and movable receiver becomes of interest. The transmitter becomes one fixed focus of the ellipsoidal wavefronts and the receiver becomes the other focus.

The transform we now study is motivated by this SAR transform. It is an elliptical Radon transform with one focus fixed on the ground and the other moving along the horizontal axis. For the SAR transform, the transmitter and receiver would be above the ground. From now on, we will let $X = \mathbb{R}^2$ and denote points in X as (x_1, x_2). We let

$$Y_o = \{(s, L) : L > |s|\} \tag{1}$$

and we parameterize the ellipse with foci $(0,0)$ and $(s,0)$ and major diameter L by

$$E_o(s,L) = \{x \in \mathbb{R}^2 : |x| + |x - (s,0)| = L\} \text{ for } (s,L) \in Y_o.$$

The restriction $L > |s|$ in the definition of Y_o is required because the major diameter must be longer than the distance between the foci.

The integral geometry problem that we are interested in is recovery of f from

$$\mathscr{R}_o f(s,L) = \int\limits_{|x|+|x-(s,0)|=L} f(x)\mathrm{d}l(x) \text{ for } (s,L) \in Y_o.$$

Here $\mathrm{d}l$ is the arc-length measure. This transform is just the integral of f over the ellipse $E_o(s,L)$.

Example 1. Ehrenpreis's nonparametric Radon transform is defined as integrals over sets which are defined by *spreads* [13, p. 4 ff]. Spreads are foliations of space that depend on a parameter. For each fixed value of the parameter, the leaves of the foliation define manifolds the Radon transform integrates over. For all parameters, all the leaves of all the foliations are diffeomorphic copies of one manifold, such as a line, plane, ellipse, or circle. The transform $\mathscr{R}_o$ is easily put into this framework. We fix s and then, for $L > s$, the map $L \mapsto E_o(s,L)$ foliates the plane (except for the segment between the origin and s) by ellipses. For any s, the leaves of the foliations are ellipses so they are diffeomorphic.

Because of the nonuniqueness results for integrals over spheres enclosing the origin [23], we expect that the transform $\mathscr{R}_o$ is not invertible. However, we might still be able to reconstruct singularities, so we will now understand what this transform and its adjoint do to singularities by analyzing the microlocal properties of the transform $\mathscr{R}_o$ and the imaging operator $\mathscr{R}_o^* \mathscr{R}_o$ (see Remark 1).

Our first theorem is

Theorem 1. $\mathscr{R}_o$ *is a Fourier integral operator of order* $-1/2$ *with canonical relation* Λ_o *defined by*

$$\Lambda_o = \left\{ \left(s, L, -\omega \frac{x_1 - s}{\sqrt{(x_1-s)^2 + x_2^2}}, -\omega; \right. \right.$$
$$x_1, x_2, -\omega \left(\frac{x_1}{\sqrt{x_1^2 + x_2^2}} + \frac{x_1 - s}{\sqrt{(x_1-s)^2 + x_2^2}} \right),$$
$$\left. \left. -\omega \left(\frac{x_2}{\sqrt{x_1^2 + x_2^2}} + \frac{x_2}{\sqrt{(x_1-s)^2 + x_2^2}} \right) \right) \right.$$
$$\left. : \omega \neq 0, (s,L) \in Y_o, \ x \in E_o(s,L) \right\}.$$

and with global parameterization (s, x_1, x_2, ω). *The left projection* $\pi_L : \Lambda_o \to T^* Y_o \setminus \mathbf{0}$ *has a fold singularity along* $\Sigma = \{(s, x_1, 0, \omega)\}$. *The right projection* $\pi_R : \Lambda_o \to T^* X \setminus \mathbf{0}$ *has a blowdown singularity along* Σ.

For the definitions of fold and blowdown singularities we refer the reader to [24] or [25]. While we do not show this here, knowing that π_L is a fold and π_R is a blowdown has implications for the comparison of the strengths (in a Sobolev sense) of the original and added singularities discussed in Theorem 2.

Proof. We use the framework of [27, 29, 28] and introduce the *incidence relation of* $\mathscr{R}_o$. This is the set

$$Z_o = \{(s,L,x) \,:\, (s,L) \in Y_o, \; x \in E_o(s,L)\}.$$

Then by results in [27, 29] we know that $\mathscr{R}_o$ is an elliptic Fourier integral operator of order $-1/2$ associated to the Lagrangian manifold $N^*(Z_o) \setminus \mathbf{0}$ (since we will show neither π_L nor π_R maps to the zero section). Computing $N^* Z_o \setminus \mathbf{0}$ and twisting it gives the canonical relation Λ_o above. It is easy to see that (s, x_1, x_2, ω) is a global parameterization of Λ_o.

We have

$$\pi_L(s, x, \omega) = \left(s, |x| + |x - (s,0)|, -\omega \frac{x_1 - s}{\sqrt{(x_1 - s)^2 + x_2^2}}, -\omega\right).$$

Since $\omega \neq 0$, we have that $\pi_L : \Lambda_o \to T^* Y_o \setminus \mathbf{0}$. Now

$$(\pi_L)_* = \begin{pmatrix} 1 & 0 & 0 & 0 \\ * & \left(\frac{x_1}{|x|} + \frac{x_1 - s}{|x - (s,0)|}\right) & \left(\frac{x_2}{|x|} + \frac{x_2}{|x - (s,0)|}\right) & * \\ * & -\omega \frac{x_2^2}{|x - (s,0)|^3} & \omega \frac{(x_1 - s)x_2}{|x - (s,0)|^3} & * \\ 0 & 0 & 0 & -1 \end{pmatrix}$$

and

$$\det((\pi_L)_*) = \omega \frac{x_2}{|x - (s,0)|^2} \left(1 + \frac{x_1(x_1 - s) + x_2^2}{|x||x - (s,0)|}\right).$$

Lemma 1. *Under the hypothesis of Equation* (1)*,* $1 + \frac{x_1(x_1 - s) + x_2^2}{|x||x - (s,0)|} > 0$.

Proof. It is easy to see that $(x_1(x_1 - s) + x_2^2)^2 < |x|^2 |x - (s,0)|^2$ is equivalent to $x_2^2 s^2 > 0$. By the hypothesis that $L > |s|$, if $x_2 = 0$, the term $\frac{x_1(x_1 - s)}{|x_1||x_1 - s|} = 1$ for all x_1 and s, from which the lemma follows. $\square$

Therefore $\det((\pi_L)_*) = 0$ if and only if $x_2 = 0$. Also since $\mathrm{d}(\det(\pi_L)_*)$ on Σ is non-vanishing, we have that π_L drops rank by one simply on Σ.

Now it remains to show that $T\Sigma \cap \mathrm{Kernel}(\pi_L)_* = \{0\}$. This follows from the fact that, above Σ, $\mathrm{Kernel}(\pi_L)_* = \mathrm{span}(\frac{\partial}{\partial x_2})$ and $T\Sigma = \mathrm{span}(\frac{\partial}{\partial s}, \frac{\partial}{\partial x_1}, \frac{\partial}{\partial \omega})$. This concludes the proof that $\pi_L : \Lambda_o \to T^* Y_o \setminus \mathbf{0}$ has a fold singularity along Σ.

Next we consider $\pi_R : \Lambda_o \to T^* X$:

$$\pi_R(s, x, \omega) = \left(x_1, x_2, -\omega\left(\frac{x_1}{|x|} + \frac{x_1 - s}{|x - (s,0)|}\right), -\omega\left(\frac{x_2}{|x|} + \frac{x_2}{|x - (s,0)|}\right)\right).$$

We now show that $\pi_R : \Lambda_o \to T^*X \setminus \mathbf{0}$. For suppose π_R maps to the zero section, then $x_2 = 0$. Now since $L > |s|$, we have that x_1 and $x_1 - s$ have the same sign. Therefore, $\frac{x_1}{|x_1|} + \frac{x_1-s}{|x_1-s|}$ is never 0. Hence π_R never maps to the zero section.

Now

$$(\pi_R)_* = \begin{pmatrix} 0 & 1 \; 0 & 0 \\ 0 & 0 \; 1 & 0 \\ \omega \dfrac{x_2^2}{|x-(s,0)|^3} & * \; * & -\left(\dfrac{x_1}{|x|} + \dfrac{x_1-s}{|x-(s,0)|} \right) \\ -\omega \dfrac{(x_1-s)x_2}{|x-(s,0)|^3} & * \; * & \left(\dfrac{x_2}{|x|} + \dfrac{x_2}{|x-(s,0)|} \right) \end{pmatrix}$$

Since $\det((\pi_R)_*) = \det((\pi_L)_*)$, π_R drops ranks by one simply along Σ. Furthermore above Σ, since $\mathrm{Kernel}(\pi_R)_* = \mathrm{span}(\frac{\partial}{\partial s}) \subset T\Sigma$, π_R has a blowdown singularity along Σ. $\quad \square$

Next we analyze the wavefront set of the imaging operator $\mathscr{R}_o^* \mathscr{R}_o$.

Remark 1. For the composition of $\mathscr{R}_o$ with $\mathscr{R}_o^*$ to be well-defined, we have to modify $\mathscr{R}_o$ by introducing an infinitely differentiable cut-off function χ_o defined on Y_o that is identically 1 on a compact subset of Y_o and 0 outside a bigger compact subset of Y_o. In the next theorem, we assume that $\mathscr{R}_o^*$ is modified using this cut-off function χ_o.

Theorem 2. *The wavefront set of the imaging operator satisfies the following:*

$$WF(\mathscr{R}_o^* \mathscr{R}_o) \subset \Delta \cup C_1$$

where

$$\Delta := \{(x_1, x_2, \xi_1, \xi_2; x_1, x_2, \xi_1, \xi_2)\} \text{ and } C_1 := \{(x_1, x_2, \xi_1, \xi_2; x_1, -x_2, \xi_1, -\xi_2)\}.$$

Here over the point $x = (x_1, x_2)$, (ξ_1, ξ_2) consists of all non-zero multiples of the vector

$$-\nabla_x \left(|x| + |x - (s,0)| \right)$$

for all $s \in \mathbb{R}$.

Remark 2. Given a point x and a focus location $(s,0)$, a vector (ξ_1, ξ_2) as in the theorem above is a vector perpendicular to the ellipse $E_o(s,L)$ (where $L = |x| + |x - (s,0)|$) at the point x.

Note that Remark 4 in Section 3 applies to this transform and there is the left-right ambiguity for $\mathscr{R}_o^* \mathscr{R}_o$ as in the common offset case discussed in that section. The implications for imaging are the same as for Theorem 4 in the common offset case; singularities of a function f on one side of the x_1 axis can be reflected to the other side in the reconstruction $\mathscr{R}_o^* \mathscr{R}_o f$.

Proof. Using the Hörmander-Sato Lemma, we have that $WF(\mathscr{R}_o^* \mathscr{R}) \subset \Lambda_o^t \circ \Lambda_o$. The composition of these two canonical relations is given as follows:

$$\Lambda_o^t \circ \Lambda_o = \left\{ \left(x_1, x_2, -\omega\left(\frac{x_1}{|x|} + \frac{x_1 - s}{|x - (s,0)|}\right), -\omega\left(\frac{x_2}{|x|} + \frac{x_2}{|x - (s,0)|}\right); \right.\right.$$

$$\left. y_1, y_2, -\omega\left(\frac{y_1}{|y|} + \frac{y_1 - s}{|y - (s,0)|}\right), -\omega\left(\frac{y_2}{|y|} + \frac{y_2}{|y - (s,0)|}\right) \right) :$$

$$|x| + |x - (s,0)| = |y| + |y - (s,0)|$$

$$\left. \frac{x_1 - s}{|x - (s,0)|} = \frac{y_1 - s}{|y - (s,0)|} \right\}.$$

Lemma 2. *For all $s > 0$, the set of all $(x_1, x_2), (y_1, y_2)$ that satisfy*

$$|x| + |x - (s,0)| = |y| + |y - (s,0)| \tag{2}$$

$$\frac{x_1 - s}{|x - (s,0)|} = \frac{y_1 - s}{|y - (s,0)|} \tag{3}$$

necessarily satisfy the relations: $x_1 = y_1$ and $x_2 = \pm y_2$.

Proof. It is straightforward to verify for the case $s = 0$. For $s \neq 0$, we use the following coordinate change to elliptical coordinates:

$$\begin{array}{ll} x_1 = \frac{s}{2} + \frac{s}{2}\cosh\rho\cos\theta & y_1 = \frac{s}{2} + \frac{s}{2}\cosh\rho'\cos\theta' \\ x_2 = \frac{s}{2}\sinh\rho\sin\theta & y_2 = \frac{s}{2}\sinh\rho'\sin\theta' \end{array}$$

From the first equation in (2), we have, $s\cos\rho = s\cos\rho'$, which then gives $\rho = \rho'$. From the second equation in (2), we have,

$$\frac{\cosh\rho\cos\theta - 1}{\cosh\rho - \cos\theta} = \frac{\cosh\rho'\cos\theta' - 1}{\cosh\rho' - \cos\theta'}$$

Using the fact that $\cosh\rho = \cosh\rho'$ and simplifying this, we obtain, $\cos\theta = \cos\theta'$. Therefore, $\theta = 2n\pi \pm \theta'$. This then gives $\sin\theta = \pm\sin\theta'$. Now going back to (x_1, y_1) and (x_2, y_2), we have $x_1 = y_1$ and $x_2 = \pm y_2$. $\quad\square$

Now to finish the proof of the theorem, when $x = y$, $\Lambda_o^t \circ \Lambda_o \subset \Delta = \{(x, \xi; x, \xi)\}$ and when $x_1 = y_1$ and $x_2 = -y_2$, $\Lambda_o^t \circ \Lambda_o \subset C_1 = \{(x_1, x_2, \xi_1, \xi_2; x_1, -x_2, \xi_1, -\xi_2)\}$. $\quad\square$

3 Analysis of a Common Offset Elliptical Radon Transform

In this section, we consider an elliptical Radon transform over a family of ellipses in which the foci move along the x_1-axis and are spaced a constant distance apart. We parameterize the right and left foci, respectively, by

$$\gamma_T(s) = (s + \alpha, 0) \quad \text{and} \quad \gamma_R(s) = (s - \alpha, 0),$$

where $\alpha > 0$ is fixed. If this were a radar problem, then γ_T would be the location of the transmitter and γ_R would be the location of the receiver. In radar imaging, the phrase "common offset" comes from the fact that the transmitter, γ_T and receiver, γ_R are *offset* a fixed distance from each other. In the case of common offset SAR, the transmitter and receiver (the foci of an ellipsoid) are on a line $h > 0$ units above the plane to be reconstructed and they travel along a line with one behind the other.

The transform we now study is motivated by this SAR transform. It is an elliptical Radon transform in which the foci are a fixed distance apart as they move along the x_1 axis in the plane. Again, $X = \mathbb{R}^2$, and we let

$$Y_c = \{(s,L) : L > 2\alpha\} \tag{4}$$

where the subscript c refers to *common* offset. The ellipse with foci $\gamma_T(s)$ and $\gamma_R(s)$ and major diameter L is denoted

$$E_c(s,L) = \{x \in \mathbb{R}^2 : |x - \gamma_T(s)| + |x - \gamma_R(s)| = L\} \text{ for } (s,L) \in Y_c.$$

The restriction $L > 2\alpha$ is needed because the major diameter of the ellipse must be longer than the distance between the foci.

In this section, we consider the integral geometry problem of recovery of f from

$$\mathscr{R}_c f(s,L) = \int_{x \in E_c(s,L)} f(x)\mathrm{d}l(x) \text{ for } (s,t) \in Y_c \tag{5}$$

which is the integral of f over the ellipse $E_c(s,L)$ in arc-length measure. As we discussed for $\mathscr{R}_o$ in Example 1, $\mathscr{R}_c$ can be put into Ehrenpreis's framework of spreads.

This case is very closely related to the results on common offset SAR in [36], and we will state our theorems and then explain how they follow from the results in [36].

Similar to Theorem 1, our first theorem in this section shows that $\mathscr{R}_c$ is an FIO, gives its canonical relation, and the mapping properties of the left and right projections from this canonical relation.

Theorem 3. *The common offset elliptical transform $\mathscr{R}_c$ is a Fourier integral operator of order $-1/2$ with canonical relation Λ_c defined by*

$$\Lambda_c = \left\{ \left(s, L, -\omega \left(\frac{x_1 - s - \alpha}{|x - \gamma_T(s)|} + \frac{x_1 - s + \alpha}{|x - \gamma_R(s)|} \right), -\omega \right); \tag{6}$$

$$\left(x_1, x_2, -\omega \left(\frac{x_1 - s - \alpha}{|x - \gamma_T(s)|} + \frac{x_1 - s + \alpha}{|x - \gamma_R(s)|} \right), -\omega \left(\frac{x_2}{|x - \gamma_T(s)|} + \frac{x_2}{|x - \gamma_R(s)|} \right) \right)$$

$$: L = \sqrt{(x_1 - s - \alpha)^2 + x_2^2} + \sqrt{(x_1 - s + \alpha)^2 + x_2^2}, \quad \omega \neq 0 \right\}.$$

Furthermore the map λ taking (s,x_1,x_2,ω) to the point in Λ given above is a global parameterization for Λ.

Finally, the projection $\pi_L : \Lambda_c \to T^*Y_c \setminus \mathbf{0}$ has a fold along $\Sigma = \{s,x_1,0,\omega\}$ and $\pi_R : \Lambda_c \to T^*X \setminus \mathbf{0}$ has a blowdown along Σ.

Proof. The assertion (6) can be proven as in [36], but here, as in Theorem 1, we outline another proof using the framework of [27, 29, 28]. The incidence relation of $\mathscr{R}_c$ is the set

$$Z_c = \{(x,s,L) : (s,L) \in Y_c, \ x \in E_c(s,L)\}.$$

Then by results in [27, 29] we know $\mathscr{R}_c$ is an elliptic Fourier integral operator of order $-1/2$ associated to Lagrangian manifold $N^*(Z_c) \setminus \mathbf{0}$ (since we will show in the course of the proof that neither π_L nor π_R maps to the zero section). Computing $N^*(Z_c)$ and twisting it gives the canonical relation (6). This is the same as the canonical relation in [36] for $h = 0$ where h is the elevation of the transmitter and receiver above the reconstruction plane.

In the parameterization λ given in the theorem, the projection, $\pi_L : \Lambda_c \to T^*Y_c$ is given by

$$\pi_L(s,x_1,x_2,\omega) \tag{7}$$

$$= \left(s, (|x - \gamma_T(s)| + |x - \gamma_R(s)|), -\omega \left(\frac{x_1 - s - \alpha}{|x - \gamma_T(s)|} + \frac{x_1 - s + \alpha}{|x - \gamma_R(s)|} \right), -\omega \right)$$

It is clear that π_L maps to $T^*Y_c \setminus \mathbf{0}$ since $\omega \neq 0$. Now from [36], by letting $h = 0$ there, we get $\det((\pi_L)_*) = \omega x_2 \left(\frac{1}{|x-\gamma_T(s)|^2} + \frac{1}{|x-\gamma_R(s)|^2} \right) \left(1 + \frac{(x_1-s)^2 + x_2^2 - \alpha^2}{|x-\gamma_T(s)||x-\gamma_R(s)|} \right)$. It is easy to see that $((x_1 - s)^2 + x_2^2 - \alpha^2)^2 < (|x - \gamma_T(s)||x - \gamma_R(s)|)^2$ is equivalent to $4x_2^2\alpha^2 > 0$. Since $L > 2\alpha$, if $x_2 = 0$, $\frac{(x_1-s)^2 - \alpha^2}{|x_1-s-\alpha||x_1-s+\alpha|} = 1$. Therefore, $\det((\pi_L)_*) = 0$ if and only if $x_2 = 0$. Also since $d(\det(\pi_L)_*)$ on Σ is non-vanishing, we have that π_L drops rank by one simply on Σ. Now as in the proof of Theorem 1, we have that, $T\Sigma = \mathrm{span}(\frac{\partial}{\partial s}, \frac{\partial}{\partial x_1}, \frac{\partial}{\partial \omega})$ and $\mathrm{Kernel}((\pi_L)_*) = \mathrm{span}(\frac{\partial}{\partial x_2})$ above Σ. This shows that $\pi_L : \Lambda_c \to T^*Y_c \setminus \mathbf{0}$ has a fold along Σ.

Next we consider $\pi_R : \Lambda \to T^*X$. This is given by

$$\pi_R(s,x_1,x_2,\omega) \tag{8}$$

$$= \left(x_1, x_2, -\omega \left(\frac{x_1 - s - \alpha}{|x - \gamma_T(s)|} + \frac{x_1 - s - \alpha}{|x - \gamma_R(s)|} \right), -\omega \left(\frac{x_2}{|x - \gamma_T(s)|} + \frac{x_2}{|x - \gamma_R(s)|} \right) \right).$$

We now show that π_R does not map to the zero section. For π_R to map to the zero section, we must have $x_2 = 0$ and

$$\frac{x_1 - s - \alpha}{|x - \gamma_T(s)|} + \frac{x_1 - s - \alpha}{|x - \gamma_R(s)|} = 0. \tag{9}$$

Using $x_2 = 0$ in (9), we see

$$\frac{x_1 - s - \alpha}{|x_1 - s - \alpha|} + \frac{x_1 - s + \alpha}{|x_1 - s + \alpha|} = 0. \tag{10}$$

However, since $(x_1, 0)$ is on an ellipse with foci $(s - \alpha, 0)$ and $(s + \alpha, 0)$, either $x_1 < s - \alpha$ or $x_1 > s + \alpha$. Therefore, both terms in (10) are non zero and have the same sign. This shows that π_R does not map to the zero section.

Now we show that π_R has a blowdown singularity along Σ. $(\pi_R)_*$ is the same as in [36], by letting $h = 0$ there. Then as in [36], we have that $\text{Kernel}((\pi_R)_*) \subset T\Sigma$. Therefore, π_R has a blowdown singularity along Σ. $\square$

Next we consider the imaging operators $\mathscr{R}_c^* \mathscr{R}_c$ and $\mathscr{R}_c^* D \mathscr{R}_c$ where D is a differential operator on Y_c. As in the last section (see Remark 1), we modify $\mathscr{R}_c$ first by multiplying it by an infinitely differentiable cutoff function χ_c that is identically 1 in a compact subset of Y_c and 0 outside a bigger compact subset.

Theorem 4. *The wavefront sets of $\mathscr{R}_c^* \mathscr{R}_c$ and $\mathscr{R}_c^* D \mathscr{R}_c$ satisfy the following:*

$$WF(\mathscr{R}_c^* \mathscr{R}_c) \subset \Delta \cup C_1 \tag{11}$$

$$WF(\mathscr{R}_c^* D \mathscr{R}_c) \subset \Delta \cup C_1 \tag{12}$$

where

$$\Delta := \{(x_1, x_2, \xi_1, \xi_2; x_1, x_2, \xi_1, \xi_2)\} \text{ and } C_1 := \{(x_1, x_2, \xi_1, \xi_2; x_1, -x_2, \xi_1, -\xi_2)\}.$$

Here, over the point $x = (x_1, x_2)$, (ξ_1, ξ_2) consists of all non-zero multiples of the vector

$$-\nabla_x (|x - \gamma_T(s)| + |x - \gamma_R(s)|)$$

for all $s \in \mathbb{R}$.

We include the differential operator D in (12) because we will discuss a reconstruction algorithm using this type of operator in Section 4.

Remark 3. Similar to Remark 2, note that given a point x and foci locations $\gamma_T(s)$ and $\gamma_R(s)$, a vector (ξ_1, ξ_2) as in the theorem above is a vector perpendicular to the ellipse $E_c(s, L)$ where $(L = |x - \gamma_T(s)| + |x - \gamma_R(s)|)$ at the point x.

Remark 4. Theorem 4 describes the added singularities in any reconstruction algorithm $\mathscr{R}_c^* D \mathscr{R}_c f$. Let f be a function of compact support in X. Using (12) one may infer [31] that

$$WF(\mathscr{R}_c^* D \mathscr{R}_c)(f) \subset (\Delta \circ WF(f)) \cup (C_1 \circ WF(f)).$$

Now,

$$\Delta \circ WF(f) = WF(f) \tag{13}$$

and

$$C_1 \circ WF(f) = \{(x_1, -x_2, \xi_1, -\xi_2) : (x_1, x_2, \xi_1, \xi_2) \in WF(f)\}. \qquad (14)$$

Therefore, the reconstruction operator $\mathscr{R}_c^* D \mathscr{R}_c f$ will show singularities of f by (13). However, the operator will also put singularities at the mirror points with respect to the x_1 axis. This is demonstrated by (14) because a singularity above the point (x_1, x_2) can cause a singularity above $(x_1, -x_2)$. We will observe this so called *left-right ambiguity* in our reconstructions in Section 4.2.

Proof. The proof is similar to the one give in [36]. Since we use a slightly different coordinate system, we will give it for completeness.

By Hörmander-Sato Lemma, we have that $WF(\mathscr{R}_c^* \mathscr{R}_c) \subset \Lambda_c^t \circ \Lambda_c$, where

$$\Lambda_c^t \circ \Lambda_c =$$

$$\left\{ \left(x_1, x_2, -\omega \left(\frac{x_1 - s - \alpha}{|x - \gamma_T(s)|} + \frac{x_1 - s + \alpha}{|x - \gamma_R(s)|} \right), -\omega \left(\frac{x_2}{|x - \gamma_T(s)|} + \frac{x_2}{|x - \gamma_R(s)|} \right) \right); \right.$$

$$\left(y_1, y_2, -\omega \left(\frac{y_1 - s - \alpha}{|y - \gamma_T(s)|} + \frac{y_1 - s + \alpha}{|y - \gamma_R(s)|} \right), -\omega \left(\frac{y_2}{|y - \gamma_T(s)|} + \frac{y_2}{|y - \gamma_R(s)|} \right) \right) :$$

$$|x - \gamma_T(s)| + |x - \gamma_R(s)| = |y - \gamma_T(s)| + |y - \gamma_R(s)|,$$

$$\left. \frac{x_1 - s - \alpha}{|x - \gamma_T(s)|} + \frac{x_1 - s + \alpha}{|x - \gamma_R(s)|} = \frac{y_1 - s - \alpha}{|y - \gamma_T(s)|} + \frac{y_1 - s + \alpha}{|y - \gamma_R(s)|}, \quad \omega \neq 0 \right\}.$$

We now obtain a relation between (x_1, x_2) and (y_1, y_2). This is given by the following lemma.

Lemma 3. *For all s, the set of all (x_1, x_2), (y_1, y_2) that satisfy*

$$|x - \gamma_T(s)| + |x - \gamma_R(s)| = |y - \gamma_T(s)| + |y - \gamma_R(s)|, \qquad (15)$$

$$\frac{x_1 - s - \alpha}{|x - \gamma_T(s)|} + \frac{x_1 - s + \alpha}{|x - \gamma_R(s)|} = \frac{y_1 - s - \alpha}{|y - \gamma_T(s)|} + \frac{y_1 - s + \alpha}{|y - \gamma_R(s)|}. \qquad (16)$$

necessarily satisfy the following relations: $x_1 = y_1$ and $x_2 = \pm y_2$.

Proof. In order to show this, we use the following change of coordinates:

$$x_1 = s + \alpha \cosh \rho \cos \theta \quad y_1 = s + \alpha \cosh \rho' \cos \theta'$$
$$x_2 = \alpha \sinh \rho \sin \theta \qquad y_2 = \alpha \sinh \rho' \sin \theta'$$

Using this change of coordinates, we have

$$|x - \gamma_T(s)| = \alpha(\cosh \rho - \cos \theta), \quad |x - \gamma_R(s)| = \alpha(\cosh \rho + \cos \theta),$$
$$\frac{x_1 - s - \alpha}{|x - \gamma_T(s)|} = \frac{\cosh \rho \cos \theta - 1}{\cosh \rho - \cos \theta}, \quad \frac{x_1 - s + \alpha}{|x - \gamma_R(s)|} = \frac{\cosh \rho \cos \theta + 1}{\cosh \rho + \cos \theta}. \qquad (17)$$

The terms involving y are obtained similarly. Now (15) and (16) transform as follows:

$$2\cosh\rho = 2\cosh\rho'$$

$$\frac{\cosh\rho\cos\theta - 1}{\cosh\rho - \cos\theta} + \frac{\cosh\rho\cos\theta + 1}{\cosh\rho + \cos\theta} = \frac{\cosh\rho'\cos\theta' - 1}{\cosh\rho' - \cos\theta'} + \frac{\cosh\rho'\cos\theta' + 1}{\cosh\rho' + \cos\theta'}.$$

Using the first equality in the second equation, we have

$$\frac{\cos\theta}{\cosh^2\rho - \cos^2\theta} = \frac{\cos\theta'}{\cosh^2\rho - \cos^2\theta'}.$$

This gives $\cos\theta = \cos\theta'$. Therefore, $\theta = 2n\pi \pm \theta'$, which then gives $\sin\theta = \pm\sin\theta'$. Therefore, in terms of (x_1, x_2) and (y_1, y_2), we have $x_1 = y_1$ and $x_2 = \pm y_2$. □

Now to finish the proof of the theorem, when $x_1 = y_1$ and $x_2 = y_2$, there is contribution to $WF(\mathscr{R}_c^*\mathscr{R}_c)$ contained in the diagonal set $\Delta := \{(x_1, x_2, \xi_1, \xi_2; x_1, x_2, \xi_1, \xi_2)\}$ and when $x_1 = y_1$ and $x_2 = -y_2$, we have a contribution to $WF(\mathscr{R}_c^*\mathscr{R}_c)$ contained in C_1, where $C_1 := \{(x_1, x_2, \xi_1, \xi_2; x_1, -x_2, \xi_1, -\xi_2)\}$. Finally note that introducing a differential operator D does not add any new singularities and so the same proof holds for the analysis of $WF(\mathscr{R}_c^*D\mathscr{R}_c)$. This completes the proof of the theorem. □

4 Our Algorithm and Reconstructions for the Common Offset Elliptical Radon Transform

In this section we describe the authors' algorithm and the refinements and implementation from [38] for the common-offset ellipse problem that was discussed in Section 3. Recall that the forward operator $\mathscr{R}_c$ and its dual $\mathscr{R}_c^*$ are both of order $-1/2$. Our reconstruction operator is

$$\Lambda(f) = \mathscr{R}_c^*(\chi_c D(\mathscr{R}_c(f))) \tag{18}$$

where D is a well-chosen second-order differential operator and χ_c is a compactly supported cut off in L. Therefore, Λ is an operator of order one so it emphasizes boundaries and other singularities.

One includes the cutoff function χ_c because $\mathscr{R}_c(f)$ does not have compact support in general, even if f has compact support. Therefore, one cannot evaluate $\mathscr{R}_c^*$ on $\mathscr{R}_c(f)$ in general, without this cutoff. We will provide more details about χ_c and the differential operator D later in this section but for the moment we will discuss this general type of algorithm.

An algorithm like (18) is called a derivative-backprojection operator because it takes a derivative and then takes some type of dual operator, a so-called backprojection operator. Such an algorithm will, typically, reconstruct singularities of the object, such as jumps at boundaries. It will image shapes and locations of objects rather than density values, and it is not an inversion method. Backprojection algo-

rithms typically use other filters besides derivatives and such algorithms have been considered in the context of bistatic SAR imaging in [57].

Therefore, researchers need to understand which singularities the algorithm reconstructs, which singularities are not imaged, and which singularities can be added to the reconstruction by the algorithm. This is one reason microlocal analysis and theorems in Section 3 are important.

Derivative-backprojection algorithms are useful in many problems, in particular when there is no inversion formula, when there is limited data, and when one is interested only in shapes, not density values.

The earliest modern tomography algorithm of this type is Lambda tomography, which was independently developed by Smith and Vainberg [55] (see [15, 14] for the state of the art). This algorithm is for planar X-ray tomography and it is useful in medical [14] and industrial tomography (e.g., [49]). The planar Lambda operator is an elliptic pseudodifferential operator, so the reconstruction shows all singularities. However, in limited angle tomography some singularities can be invisible, as in electron microscopy [51].

In three-dimensional tomography problems, singularities can be spread, and artifacts can be created that are of the same strength as the original singularities. This occurs in local backprojection algorithms for cone beam 3-D CT (e.g., [39, 34]), and this was proven in [21] (see [25] for general admissible line complexes on manifolds). A derivative-backprojection reconstruction algorithm was developed for slant-hole SPECT in [50]. It was shown in [20] that if one chooses the right differential operator D, then the added singularities are suppressed in relation to the genuine singularities, and so they are less obvious in the reconstruction. Unfortunately, $\mathscr{R}_c$ spreads singularities in a more complicated way than the slant-hole SPECT transform and it is an open problem to find a differential operator to globally decrease the strength of the added singularities.

4.1 Our algorithm

The choices of the differential operator D and of the cutoff function χ_c in our reconstruction operator Λ (18) are important, and we describe them in this section.

It is shown in [38] that the operator

$$D = -\frac{\partial^2}{\partial L^2} \tag{19}$$

gives better reconstructions than the operator $-\frac{\partial^2}{\partial s^2}$. Boundaries are imaged more clearly as we will now explain using Fig. 1. Let f be the characteristic function of the ball in Fig. 1 and let x be the point of tangency of the ellipse in the top picture in Fig. 1. One can see from the lower left image in Fig. 1 that because the ellipse moves into the ball as L is increased, and the integral, $\mathscr{R}_c f(s, L)$, increases from zero like a square root function. Therefore $\frac{\partial^2}{\partial L^2} \mathscr{R}_c f$ will be unbounded at this ellipse.
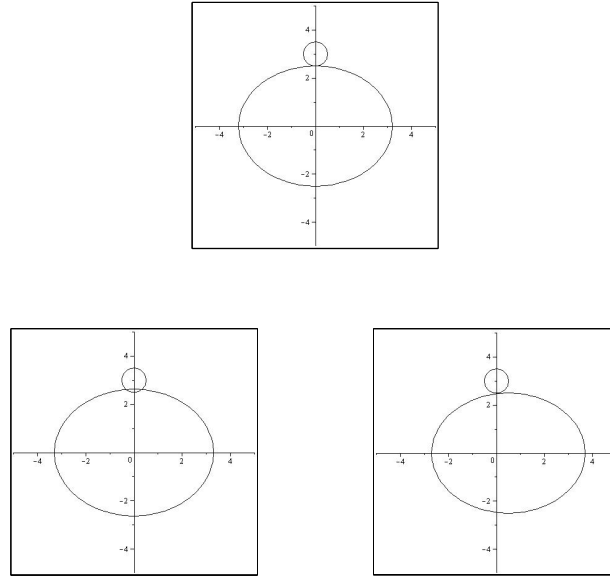
Fig. 1 The top figure shows the ellipse $E(s,L)$ tangent to a ball at the top point of the minor axis. The figure on the lower left shows the ellipse if L is increased slightly, and the ellipse intersects the ball. The figure on the lower right shows the ellipse if s is increased slightly. In this case, the ellipse remains outside the ball.

The reconstruction operator, $\mathscr{R}_c^* \frac{\partial^2}{\partial L^2} \mathscr{R}_c f$, averages $\frac{\partial^2}{\partial L^2} \mathscr{R}_c f$ all ellipses through x. Therefore, the reconstruction at x will be large.

However, movement in the s (horizontal) direction keeps the ellipse outside of the ball, so $\mathscr{R}_c f(s,L)$ remains zero and $\frac{\partial^2}{\partial s^2} \mathscr{R}_c f$ will be zero at this ellipse. For ellipses nearby, the s derivative of the data will also be small. Therefore, the reconstruction operator, $\mathscr{R}_c^* \frac{\partial^2}{\partial s^2} \mathscr{R}_c f$, which averages this derivative on all ellipses through x will be small. These horizontal boundaries were almost invisible in the $\partial^2/\partial s^2$ reconstructions in [38]. If the ellipse was tangent at another point, then as s increased, the ellipse could intersect the ball, but $\mathscr{R}_c f$ would, in general, increase from zero more slowly than if L were increased and so the derivative in s would be smaller than the derivative in L.

4.2 Reconstructions

We now present reconstructions of the characteristic function of a ball of radius $1/2$ and centered at $(0,1)$: $B((0,1),1/2)$. The backprojection $\mathscr{R}_c^*$ is implemented using

the trapezoidal rule and the derivative D is implemented using a central second difference. The common offset is $d = 1/4$ ($\alpha = 1/8$). Details are in the second author's senior honors thesis [38].

We will analyze both types of artifacts in the reconstructions, those caused by the left-right ambiguity and those caused by the limited range on s.

As noted in Remark 4 after Theorem 4, the reconstruction operator (18) for the common offset elliptical transform has the *left-right ambiguity*: singularities on one side of the x_1 axis are reflected on the other side in the reconstruction. This explains why our reconstructions put copies of the circle on both the right and left of the flight path. This global spreading of singularities is more difficult to decrease than the local spreading in SPECT [50, 20] and electron microscopy [51].

The second type of added singularity is the "parentheses" surrounding and tangent to the circle, and they are explained by the limited values of s or, equivalently, the support of the cutoff χ_C. The choice of cutoff function χ_c makes an important difference to the reconstruction [38]. Two parameters, $M > m > 0$ are chosen and the cutoff function $\chi_c(L)$ is supported in $[-M, M]$ and equal to one in $[-m, m]$. In this case χ_c does not need to be compactly supported on Y_c but only in L since the functions we reconstruct have compact support.

If one looks carefully at the reconstructions, one can show that the "parentheses" artifacts are parts of the boundaries of ellipses that are tangent to the circle and with $s = -M$ (for the ones "pointing" right) and with $s = M$ (for the ones "pointing" left). These are ellipses with foci at $(-3, 0)$ and $(-2.75, 0)$ tangent to the ball and two with foci at $(2.75, 0)$ and $(3, 0)$ tangent to the ball.
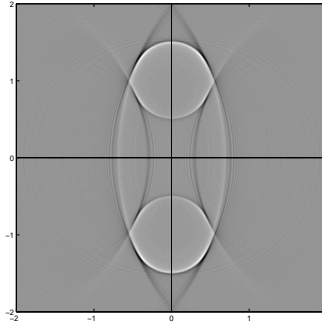
Fig. 2 Reconstruction of the ball $B((0,1), 1/2)$ using the function χ_c supported on $[-3, 3]$ and equal to 1 on $[-9/4, 9/4]$.

The authors believe there are both microlocal reasons and practical grounds for these elliptical artifacts. If the integration had been over $[-3, 3]$ without a smooth cutoff χ_c, then the operator would not have smooth kernel and that could cause the artifact because Λ would not be a smooth Fourier integral operator. However, the

algorithm includes the smooth function χ_c and there is still an artifact. In order to reduce the effect of these artifacts we changed the cutoff χ_c. In Fig. 3, the artifacts
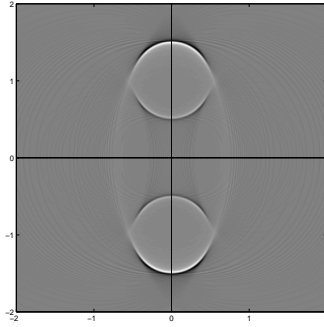
Fig. 3 Reconstruction of the ball $B((0,1),1/2)$ using the function χ_c supported on $[-3,3]$ and equal to 1 only at the origin, $[0,0]$.

caused by these ellipses are decreased but somewhat fewer singularities are visible.

Smith's implementation of Lambda tomography includes a constant term in the derivative D. This shows contours of the object because it adds a multiple of the simple backprojection; for our case it would be $\mathscr{R}_c^* \chi_c \mathscr{R}_c$. The reconstruction in Fig. 4 illustrates this, and the inside of the ball has higher "density" than the outside.
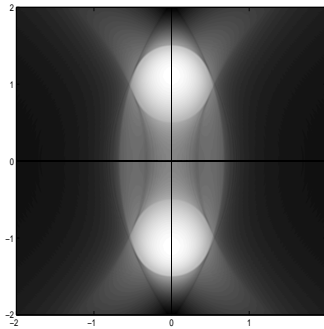
Fig. 4 Reconstruction with $D = 1 - \frac{\partial^2}{\partial L^2}$, which includes the simple backprojection as well as the derivative in L

5 Discussion

In this section, we will discuss the implications of our work for bistatic SAR, and we will suggest some open problems and conjectures.

The elliptical Radon transforms we consider in this article, while motivated by bistatic SAR imaging, are simplifications of the operators that appear in bistatic SAR. In our case, the transmitter and receiver are on the ground, and in general, in SAR, they are above the ground. The canonical relations in SAR are different from ours, but they become the same if the transmitter and receiver are on the ground. The SAR operators are also FIOs of a different order. For the common offset case with transmitter and receiver above the ground, the projections are a fold and blowdown [36], as in our case. It is easy to see that the same holds for the transform with one fixed focus above the origin and the other moving above the horizontal axis.

The appearance of ambiguities is a serious issue in SAR imaging. In the acquisition geometries we considered in this paper, we showed in Theorems 2 and 4 that there are only left-right ambiguities. We can decrease such ambiguities by focusing the antenna beam (known as beam forming) to the right or left of the flight path. However, one then images only one half of the scene and one must fly over the scene again to image the other side. In general, one needs to know the nature and structure of such ambiguities in order to decide if focusing the beam could decrease these ambiguities. For general bistatic acquisition geometries, this is an open problem. The structure of ambiguities could be very complicated in this case.

Monostatic SAR has colocated transmitter and receiver. For such SAR systems, more is known. For linear flight trajectory, a similar theorem to Theorem 3 is true, namely for that canonical relation, π_L is a fold along the set Σ at which it drops rank, and π_R is a blowdown along Σ, and Theorem 4 is also true in this case[42, 16, 17].

For linear flight paths and monostatic or bistatic SAR, it is conjectured that, without beam forming, the left-right ambiguity is intrinsic to the problem and cannot be eliminated.

However, for other flight paths, more can be done. Injectivity holds for the circular transform with centers on a curve as long as the curve is not a line or a Coxeter system of lines [1]. This suggests, but does not prove, that the general monostatic SAR transform is injective for such curves. For nonlinear flight tracks, there is a local left-right ambiguity as can be seen from reconstructions in [38]. However, these added singularities seem to be spread and look quantitatively weaker than for linear flight tracks. Felea [17] showed that for the monostatic SAR transform with circular flight tracks, one can displace added singularities far away from the image [17].

We conjecture that Felea's methods would work for the circular transform because it has the same canonical relation as the monostatic SAR transform. For the elliptical Radon transform with transmitter and receiver a fixed distance apart along a circle, the reconstruction operator is an elliptical pseudodifferential operator as long as the scene is sufficiently inside the circle [2]. This suggests that ideas in [17] might be helpful for the bistatic case with circular trajectories.

Nolan and Dowling [44] showed that if one takes monostatic data over two perpendicular linear flight paths, then the added singularities caused by the left-right

ambiguity are quantitatively weaker than the image itself. This makes sense because, when one adds the images, only the real image reinforces itself.

The authors and their colleagues will continue investigating novel flight paths and reconstruction algorithms, evaluating them using microlocal analysis as we have done in this article for the elliptical transform with one fixed focus and for the common-offset case.

References

1. Agranovsky, M., Quinto, E.T.: Injectivity sets for Radon transform over circles and complete systems of radial functions. J. Functional Anal. **139**, 383–414 (1996)
2. Ambartsoumian, G., Krishnan, V., Quinto, E.T.: The microlocal analysis of the ultrasound operator with circular source and receiver trajectory. Tech. rep., University of Texas at Arlington, University of Bridgeport, Tufts University (2011). Submitted.
3. Andersson, L.E.: On the determination of a function from spherical averages. SIAM J. Math. Anal. **19**, 214–232 (1988)
4. Boman, J.: Helgason's support theorem for Radon transforms - a new proof and a generalization, *Lecture Notes in Mathematics*, vol. 1497, pp. 1–5. Springer Verlag, Berlin, New York (1991)
5. Boman, J., Quinto, E.T.: Support theorems for real analytic Radon transforms. Duke Math. J. **55**, 943–948 (1987)
6. Cheney, M.: A mathematical tutorial on synthetic aperture radar. SIAM Rev. **43**(2), 301–312 (electronic) (2001). DOI 10.1137/S0036144500368859. URL http://dx.doi.org/10.1137/S0036144500368859.
7. Cheney, M., Borden, B.: Microlocal structure of inverse synthetic aperture radar data. Inverse Problems **19**(1), 173–193 (2003). DOI 10.1088/0266-5611/19/1/310. URL http://dx.doi.org/10.1088/0266-5611/19/1/310
8. Cheney, M., Borden, B.: Fundamentals of Radar Imaging, *CBMS-NSF Regional Conference Series in Applied Mathematics*, vol. 79. Society for Industrial and Applied Mathematics (2009)
9. Courant, R., Hilbert, D.: Methods of Mathematical Physics, vol. II. Wiley-Interscience, New York (1962)
10. D.Miller, M.O., Beylkin, G.: A new slant on seismic imaging: Migration and integral geometry. Geophysics **52**(7), 943 – 964 (1987)
11. deHoop, M., Smith, H., Uhlmann, G., van der Hilst, R.: Seismic imaging with the generalized Radon transform: A curvelet transform perspective. Inverse Problems **25** (2009). Doi:10.1088/0266-5611/25/2/025005
12. Ehrenpreis, L.: Three problems at Mount Holyoke. Contemporary Math. pp. 123–130 (2001)
13. Ehrenpreis, L.: The universality of the Radon Transform. Oxford University Press, Oxford, UK (2003)
14. Faridani, A., Finch, D., Ritman, E.L., Smith, K.T.: Local tomography, II. SIAM J. Appl. Math. **57**, 1095–1127 (1997)
15. Faridani, A., Ritman, E.L., Smith, K.T.: Local tomography. SIAM J. Appl. Math. **52**, 459–484 (1992)
16. Felea, R.: Composition of Fourier integral operators with fold and blowdown singularities. Comm. Partial Differential Equations **30**(10-12), 1717–1740 (2005). DOI 10.1080/03605300500299968. URL http://dx.doi.org/10.1080/03605300500299968

17. Felea, R.: Displacement of artefacts in inverse scattering. Inverse Problems **23**(4), 1519–1531 (2007). DOI 10.1088/0266-5611/23/4/009. URL http://dx.doi.org/10.1088/0266-5611/23/4/009

18. Felea, R., Greenleaf, A.: An FIO calculus for marine seismic imaging: folds and cross caps. Comm. Partial Differential Equations **33**(1-3), 45–77 (2008). DOI 10.1080/03605300701318716. URL http://dx.doi.org/10.1080/03605300701318716

19. Felea, R., Greenleaf, A., Pramanik, M.: An FIO calculus for marine seismic imaging, II: Sobolev estimates. Tech. rep., University of Rochester, Rochester Institute of Technology (2010). Preprint

20. Felea, R., Quinto, E.T.: The microlocal properties of the local 3-D SPECT operator. SIAM J on Math Analysis **43**(3), 1145–1157 (2011)

21. Finch, D.V., Lan, I.R., Uhlmann, G.: Microlocal Analysis of the Restricted X-ray Transform with Sources on a Curve. In: G. Uhlmann (ed.) Inside Out, Inverse Problems and Applications, *MSRI Publications*, vol. 47, pp. 193–218. Cambridge University Press (2003)

22. Funk, P.: Über eine geometrische Anwendung der Abelschen Integralgleichung. Math. Ann. **77**, 129–135 (1916)

23. Globevnik, J.: Zero integrals on circles and characterizations of harmonic and analytic functions. Trans. Amer. Math. Soc. **317**, 313–330 (1990)

24. Golubitsky, M., Guillemin, V.: Stable mappings and their singularities. Springer-Verlag, New York (1973). Graduate Texts in Mathematics, Vol. 14

25. Greenleaf, A., Uhlmann, G.: Nonlocal inversion formulas for the X-ray transform. Duke Math. J. **58**(1), 205–240 (1989). DOI 10.1215/S0012-7094-89-05811-0. URL http://dx.doi.org/10.1215/S0012-7094-89-05811-0

26. Greenleaf, A., Uhlmann, G.: Composition of some singular Fourier integral operators and estimates for restricted X-ray transforms. Ann. Inst. Fourier (Grenoble) **40**(2), 443–466 (1990)

27. Guillemin, V.: Some remarks on integral geometry. Tech. rep., MIT (1975)

28. Guillemin, V.: On some results of Gelfand in integral geometry. Proceedings Symposia Pure Math. **43**, 149–155 (1985)

29. Guillemin, V., Sternberg, S.: Geometric asymptotics. American Mathematical Society, Providence, R.I. (1977). Mathematical Surveys, No. 14

30. Helgason, S.: The Radon transform on Euclidean spaces, compact two-point homogeneous spaces and Grassmann manifolds. Acta Math. **113**, 153–180 (1965)

31. Hörmander, L.: The analysis of linear partial differential operators. I. Classics in Mathematics. Springer-Verlag, Berlin (2003). Distribution theory and Fourier analysis, Reprint of the second (1990) edition [Springer, Berlin; MR1065993 (91m:35001a)]

32. Horne, A., Yates, G.: Bistatic synthetic aperture radar. In: Proceedings of IEEE Radar Conference, pp. 6 – 10 (2002)

33. John, F.: Plane waves and spherical means applied to partial differential equations. Interscience, New York (1966)

34. Katsevich, A.: Improved Cone Beam Local Tomography. Inverse Problems **22**, 627–643 (2006)

35. Krishnan, V.P.: A support theorem for the geodesic ray transform on functions. J. Fourier Anal. Appl. **15**(4), 515–520 (2009). DOI 10.1007/s00041-009-9061-5. URL http://dx.doi.org/10.1007/s00041-009-9061-5

36. Krishnan, V.P., Quinto, E.T.: Microlocal aspects of bistatic synthetic aperture radar imaging. Inverse Problems and Imaging **5**, 659–674 (2011).

37. Krishnan, V.P., Stefanov, P.: A support theorem for the geodesic ray transform of symmetric tensor fields. Inverse Problems and Imaging **3**(3), 453–464 (2009)

38. Levinson, H.: Algorithms for Bistatic Radar and Ultrasound Imaging, Senior Honors Thesis with Highest Thesis Honors, (2011), Tufts University.

39. Louis, A.K., Maaß, P.: Contour reconstruction in 3-D X-Ray CT. IEEE Trans. Medical Imaging **12**(4), 764–769 (1993)

40. Mensah, S., Franceschini, E.: Near-field ultrasound tomography. J. Acoust. Soc. Am. **121**(3), 1423 –1433 (2007). DOI 10.1109/TIP.2009.2039662

41. Nolan, C.J., Cheney, M.: Synthetic aperture inversion. Inverse Problems **18**(1), 221–235 (2002). DOI 10.1088/0266-5611/18/1/315. URL http://dx.doi.org/10.1088/0266-5611/18/1/315
42. Nolan, C.J., Cheney, M.: Microlocal analysis of synthetic aperture radar imaging. J. Fourier Anal. Appl. **10**(2), 133–148 (2004). DOI 10.1007/s00041-004-8008-0. URL http://dx.doi.org/10.1007/s00041-004-8008-0
43. Nolan, C.J., Cheney, M., Dowling, T., Gaburro, R.: Enhanced angular resolution from multiply scattered waves. Inverse Problems **22**(5), 1817–1834 (2006). DOI 10.1088/0266-5611/22/5/017. URL http://dx.doi.org/10.1088/0266-5611/22/5/017
44. Nolan, C.J., Dowling, T.: Private Communication.
45. Nolan, C.J., Symes, W.W.: Global solution of a linearized inverse problem for the wave equation. Comm. Partial Differential Equations **22**(5-6), 919–952 (1997). DOI 10.1080/03605309708821289. URL http://dx.doi.org/10.1080/03605309708821289
46. Quinto, E.T.: The dependence of the generalized Radon transform on defining measures. Trans. Amer. Math. Soc. **257**, 331–346 (1980)
47. Quinto, E.T.: Singularities of the X-ray transform and limited data tomography in $\mathbb{R}^2$ and $\mathbb{R}^3$. SIAM J. Math. Anal. **24**, 1215–1225 (1993)
48. Quinto, E.T.: Support Theorems for the Spherical Radon Transform on Manifolds. International Mathematics Research Notices **2006**, 1–17 (2006). Article ID = 67205
49. Quinto, E.T.: Local Algorithms in Exterior Tomography. Journal of Computational and Applied Mathematics **199**, 141–148 (2007)
50. Quinto, E.T., Bakhos, T., Chung, S.: A local algorithm for Slant Hole SPECT. In: Mathematical Methods in Biomedical Imaging and Intensity-Modulated Radiation Therapy (IMRT), pp. 321–348. Centro De Georgi, Pisa, Italy (2008). CRM Series, Volume 7
51. Quinto, E.T., Öktem, O.: Local tomography in electron microscopy. SIAM J. Appl. Math. **68**, 1282–1303 (2008)
52. Stefanov, P.: Microlocal approach to tensor tomography and boundary and lens rigidity. Serdica Math. J. **34**(1), 67–112 (2008)
53. Stefanov, P., Uhlmann, G.: Boundary rigidity and stability for generic simple metrics. J. Amer. Math. Soc. **18**(4), 975–1003 (electronic) (2005). DOI 10.1090/S0894-0347-05-00494-7. URL http://dx.doi.org/10.1090/S0894-0347-05-00494-7
54. Vaidyanathan, R.S., Lewis, M., Ambartsoumian, G., Aktosun, T.: Reconstruction algorithms for interior and exterior spherical Radon transform-based ultrasound imaging. In: Proceedings of SPIE, v. 7265, Medical Imaging 2009: Ultrasonic Imaging and Signal Processing, pp. 72,651I 1– 8 (2009)
55. Vainberg, E., Kazak, I.A., Kurozaev, V.P.: Reconstruction of the internal three-dimensional structure of objects based on real-time integral projections. Soviet Journal of Nondestructive Testing **17**, 415–423 (1981)
56. Volchkov, V.V.: Integral geometry and convolution equations. Kluwer Academic Publishers, Dordrecht (2003)
57. Yarman C.E, Yazıcı B., Cheney, M.: Bistatic Synthetic Aperture Radar Imaging with Arbitrary Trajectories. IEEE Transactions on Image Processing, **17**(1), 84–93, (2008).
58. Zalcman, L.: Offbeat Integral Geometry. Amer. Math. Monthly **87**, 161–175 (1980)